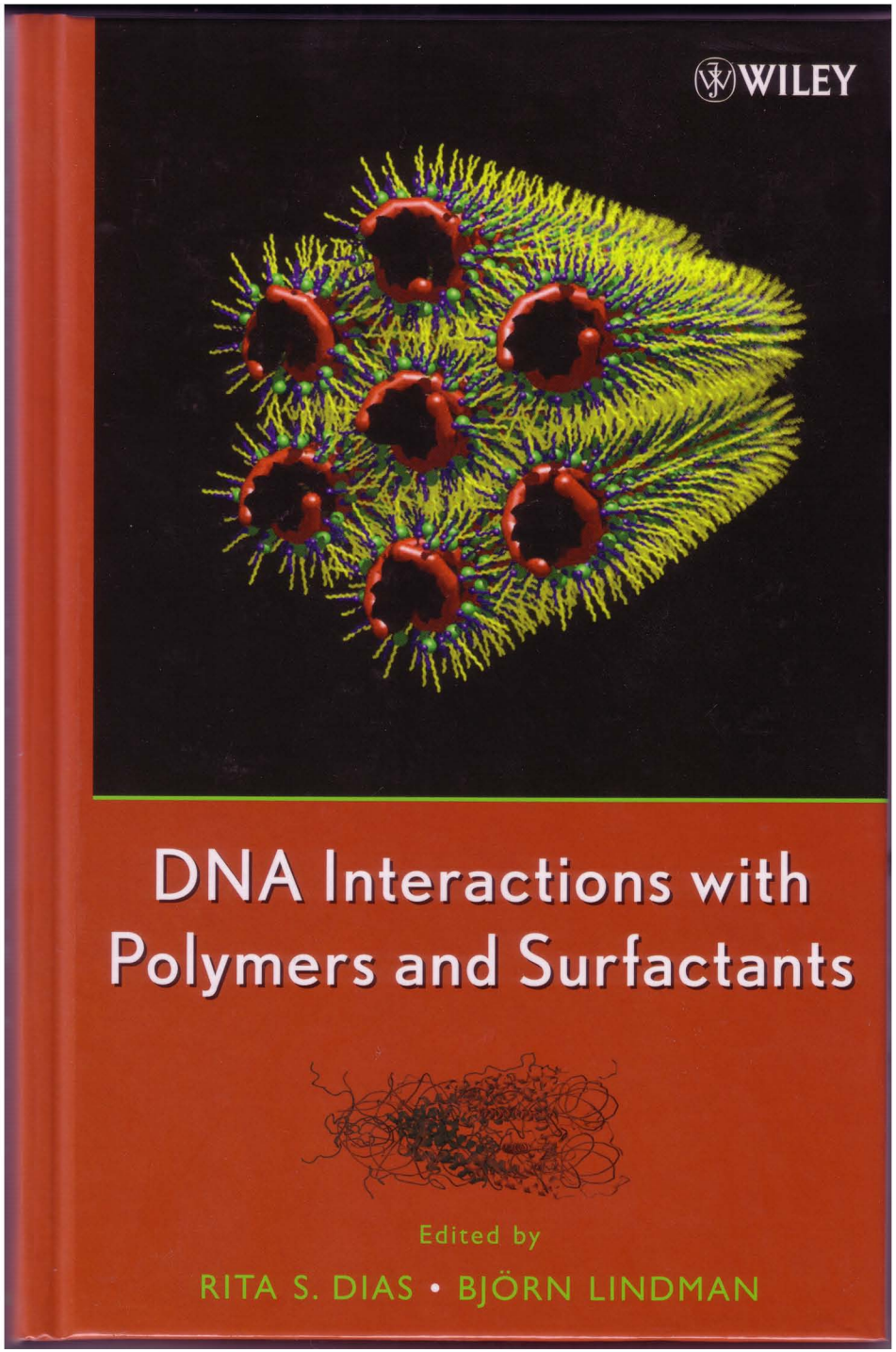

CHAPTER 16

Lipid–DNA Interactions: Structure–Function Studies of Nanomaterials for Gene Delivery

KAI K. EWERT, CHARLES E. SAMUEL, and CYRUS R. SAFINYA

16.1 INTRODUCTION

The interaction of DNA with oppositely charged cosolutes such as cationic lipids and polymers has attracted a large amount of scientific interest ever since the seminal finding of Felgner et al. [1] that cationic lipids may be used to transfer DNA into mammalian cells [2–7]. Gene therapy, the use of DNA (genes) as a drug, promises cures for a wide variety of diseases. These include inherited diseases, cancers, cardiovascular diseases, and many others. However, while a large number of clinical trials of gene therapy are currently ongoing worldwide [8,9], delivery of the desired DNA remains a big challenge. The use of genetically modified viruses still accounts for the majority of clinical trials and has yielded the first successful cure by gene therapy [10]. But these "viral methods" have also come under increased scrutiny because of a few recent setbacks that have highlighted the safety drawbacks of viral vectors [11–13]. Viruses activate the immune system and they have led to insertional mutagenesis in oncogenes. There is a small but finite chance of the viral vector becoming viable again, and their capacity is limited to about 40,000 base pairs. Therefore nonviral vectors for gene delivery have generated increasing interest [2–7]. These vectors are formed by the self-assembly of DNA and cationic lipids (CL) or polymers, and thus they impose no limit on the size of the DNA that may be delivered [14]. In fact cationic lipid vectors have been used to transfer fractions of a human artificial chromosome—at a size of about 1 million base pairs—into cells [15]. In addition cationic lipid vector are much easier to prepare than viruses. Commercial lipid formulations are available and are used widely for transfection of cells in culture.

DNA Interactions with Polymers and Surfactants Edited by Rita Dias and Björn Lindman

However, to be a viable vector for applications in gene therapy, the efficiency of nonviral vectors needs to be improved.

In this chapter we present an overview of work aimed at determining the mechanisms of transfection of cationic lipid (CL)–DNA complexes and how their structures and physicochemical parameters affect their transfection mechanism and efficiency. Such knowledge is expected to yield the basis for a rational optimization of CL–DNA vectors. The in vitro studies described here apply directly to a transfection efficiency (TE) optimization in ex vivo cell transfection, where cells are removed and returned to patients after transfection.

CL–DNA complexes readily form with a large variety of lipids. This ease of preparation and the variability of the lipid composition constitute two of the main advantages of CL vectors. Typically a mixture of at least two lipids is used. One is a cationic lipid, and the other one, sometimes called a "helper lipid," is a neutral lipid. The structures of most lipids mentioned in this chapter are shown in Figure 16.1 and Table 16.1. As neutral lipids, 1,2-dioleoyl-sn-glycerophosphatidylethanolamine (DOPE) and 1,2-dioleoyl-sn-glycerophosphatidylcholine (DOPC) were employed. DOPE is one of the most popular neutral lipids currently in use in gene therapy applications of CLs. DOTAP (2,3-dioleoyloxypropyltrimethylammonium chloride) is a commercially available, standard cationic lipid. The MVLs and PEG-lipids were synthesized in our group [16–20].

16.2 FORMATION AND STRUCTURES OF CL–DNA COMPLEXES

In this section we discuss the findings relevant to understanding the formation, nanostructure, and thermodynamic stability of CL–DNA complexes.

In aqueous solutions both DNA and cationic lipid assemblies (liposomes or micelles) are associated with their respective counterions. The high charge density of DNA actually results in "counterion condensation": in its solution structure, the bare length between negative phosphate groups on the DNA backbone is equal to $l_0 = 1.7$ Å. This is less than the Bjerrum length in water $l_B\,\varepsilon(\equiv e^2/\varepsilon_w k_B T) = 7.1$ Å, with the dielectric constant of water $\varepsilon_w = 80$. The Bjerrum length corresponds to the distance where the Coulomb energy between two unit charges is equal to the thermal energy $k_B T$. Under these conditions a mean-field nonlinear Poisson–Boltzmann analysis shows that positive counterions will condense on the DNA backbone until the Manning parameter $\xi \equiv l_B/l_0^*$ approaches unity [21]. Here l_0^* is the renormalized distance between the negative charges after counterion condensation.

A similar analysis shows that near the surface of a positively charged membrane, for example, the cationic liposome surface, nearly half of the negative counterions are contained within the Gouy–Chapman length $l_{G\text{-}C} \equiv e/2\pi l_B \sigma_M$. Here σ_M is the charge density of the lipid membrane [22].

Combining DNA and cationic lipid allows the charges of the lipid head-group to neutralize the phosphate groups on the DNA. This replaces and releases the tightly bound counterions of both lipid and DNA into solution (Figure 16.2, top). The resulting gain of translational entropy by the counterions is the driving force for higher order

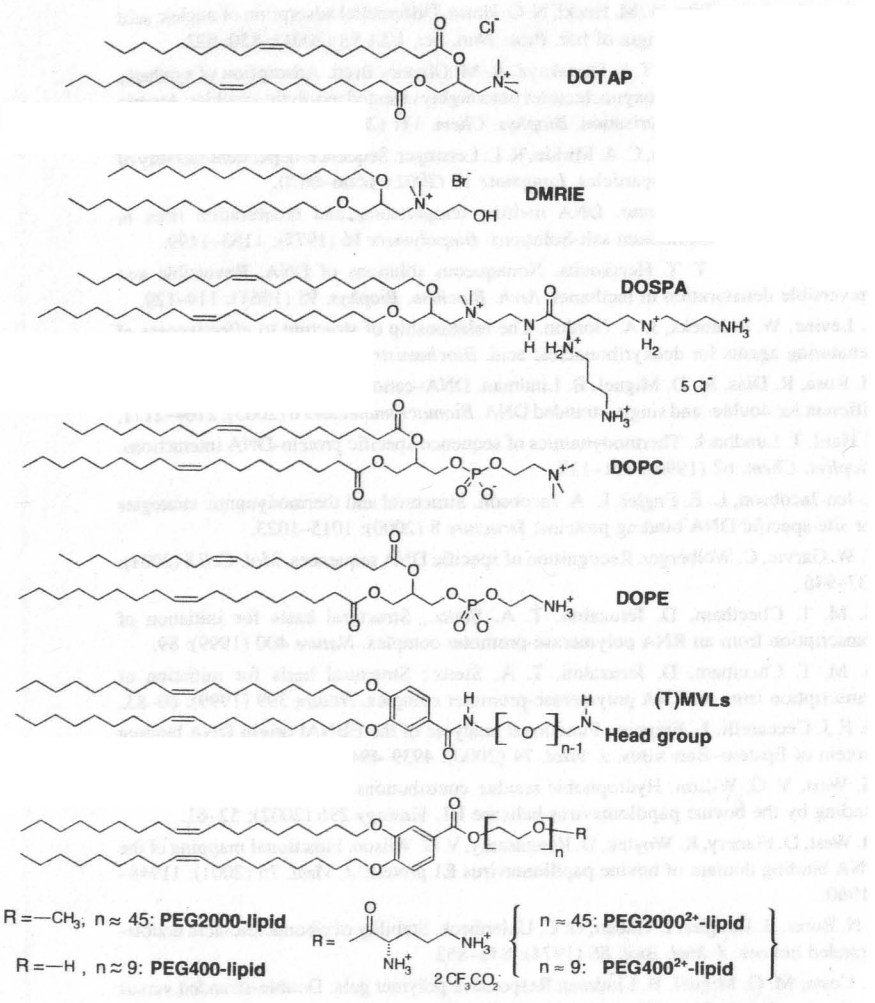

Figure 16.1 Chemical structures and abbreviated names of cationic and neutral lipids mentioned in this chapter. See Table 16.1 for Head-Group structures, spacer lengths, and lipid names of the (T)MVLs.

self-assembly into CL–DNA complexes [23–25]. We use the term "bound counterions" in a loose form: the counterions near the macromolecular surfaces are "bound" and yet remain in a fully hydrated state. Thus there is no change in the entropy of water molecules when "bound counterions" are released into solution.

Mesoscopically the mixing of cationic lipid and DNA results in their spontaneous self-assembly into small globular particles (0.2 μm diameter) of CL–DNA complexes.

TABLE 16.1 Abbreviated Names and Spacer Lengths of Newly Synthesized Multivalent Cationic Lipids, their Charge and the Chemical Structures of their Head-Groups

Lipid name	Charge / e		Headgroup structure
	Z_{max} [a]	Z_{exp} [b]	
MVL2 (n=1)	+2	2.0 ± 0.1 [c]	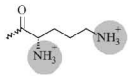
MVL3 (n=1)	+3	2.5 ± 0.1 [c]	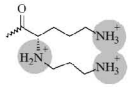
MVL5 (n=1) TMVL5 (n=3)	+5	4.5 ± 0.1 [c]	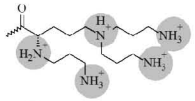
MVLG2 (n=1) TMVLG2 (n=3)	+ 4	3.98 ± 0.24 [d]	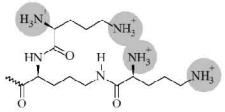
MVLBG1 (n=1) TMVLBG1 (n=3)	+ 8	8.00 ± 0.10 [d]	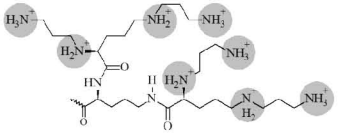
MVLG3 (n=1) TMVLG3 (n=3)	+ 8	7.93 ± 0.26 [d]	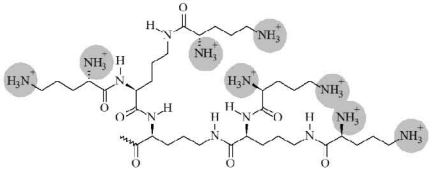
MVLBG2 (n=1) TMVLBG2 (n=3)	+ 16	15.9 ± 1.0	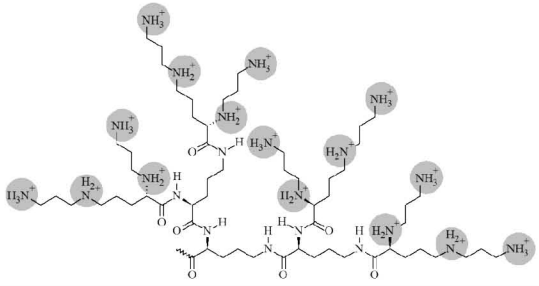

[a] Charge at full protonation
[b] Charge in complex, determined by an ethidium bromide displacement assay.
[c] See [18]
[d] See [20]

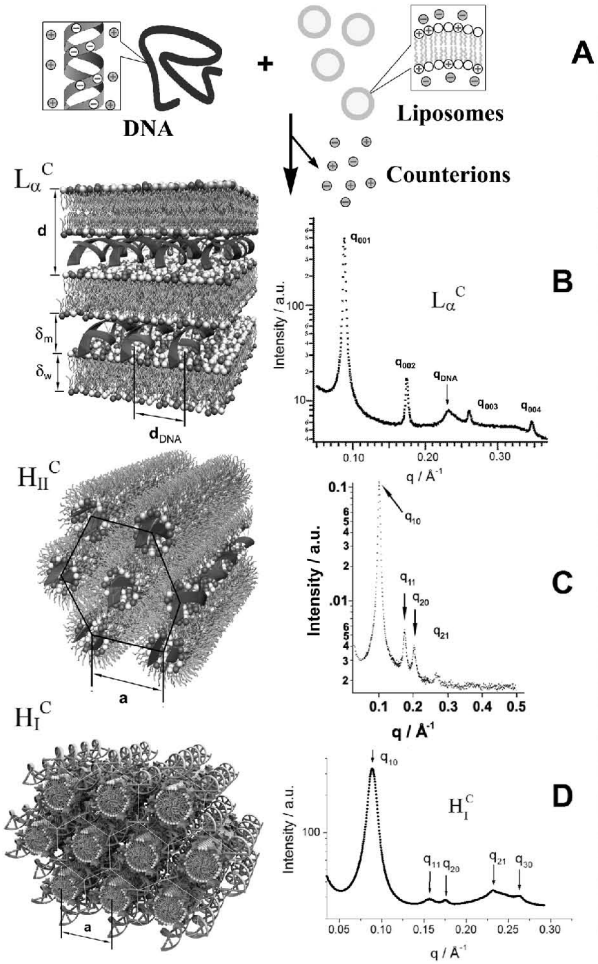

Figure 16.2 (*A*) Schematic of the formation of CL–DNA complexes from liposomes and DNA. The release of tightly bound counterions is the driving force for the self-assembly process. (*B–D*) Schematic depictions of the nanoscale interior structure of the three known phases of CL–DNA complexes: lamellar (L_α^C), inverted hexagonal (H_{II}^C), and hexagonal (H_I^C) phases. Also shown are characteristic X-ray scattering patterns for the three phases. (Reprinted in part with permission from [19,29]. H_I^C phase images © 2006 American Chemical Society)

This self-assembly has been shown for a large variety of lipids by way of differential interference contrast microscopy [14,17–19]. Fluorescence microscopy reveals the presence of both lipid and DNA within these particles. Depending on the complex composition (i.e., surface charge) and the solution conditions (e.g., salt content), the

primary particles may aggregate further over time. The effects of varying the two main compositional parameters, lipid–DNA charge ratio and ratio of neutral to cationic lipid, will, be discussed, below.

Synchrotron X-ray diffraction has yielded insight into the nanoscale structure of self-assembled CL–DNA complexes. The three phases of CL–DNA complexes reported to date are shown in Figure 16.2, together with examples of their characteristic X-ray scattering patterns. The lamellar (L_α^C) phase is the most commonly observed structure. The sharp, evenly spaced 00L peaks (marked q_{001}, q_{002}, ...) result from the layered structure of the CL–DNA complexes with $d = \delta_m + \delta_w = 2\pi/q_{001}$. Here δ_m is the membrane thickness, which can be measured independently via X-ray diffraction of multilamellar lipid assemblies in the absence of DNA. The remaining water layer thickness $\delta_w = d - \delta_m$ typically equals about 25 Å, the thickness required for a monolayer of DNA in its hydrated B-form. The broad peak visible between the 002 and 003 reflections is a DNA–DNA correlation peak and yields the average interaxial distance between the DNA rods as $d_{DNA} = 2\pi/q_{DNA}$.

The sandwiched DNA forms an array of chains that uniformly covers the available lipid area. Thus d_{DNA} is a simple function of the lipid–DNA charge ratio ρ_{chg} (see also below) and has been found to range from roughly 25 Å at high membrane charge densities—where the DNA rods are nearly touching—to roughly 55 Å at low membrane charge densities [14,26–28]. The lamellar L_α^C phase of CL–DNA complexes is a novel hybrid liquid crystalline phase: the lipids form a three-dimensional smectic phase while the DNA rods between the lipid bilayers from a two-dimensional smectic phase.

At certain compositions, CL–DNA complexes containing the popular helper lipid DOPE and the cationic lipid DOTAP have been shown to form the inverted hexagonal (H_{II}^C) phase of CL–DNA complexes [29]. The nanoscale internal structure and typical X-ray scattering pattern of this phase are also shown in Figure 16.2. DOPE differs from DOPC only by possessing an ammonium group in place of a trimethylammonium group. However, the weaker hydration of this group reduces the headgroup size of DOPE significantly, resulting in a cone-like molecular shape. Thus DOPE confers a negative curvature to membranes, whereas DOTAP and DOPC induce a zero (flat) spontaneous curvature. The negative curvature favors the formation of the inverse micelles present in the columnar liquid-crystalline H_{II}^C structure, which is observed in the DOTAP/DOPE system when the weight fraction of DOPE, $\Phi_{DOPE} \equiv \text{weight}_{DOPE}/(\text{weight}_{DOPE} + \text{weight}_{DOTAP})$, is larger than roughly 0.65 [29,30]. The DNA molecules are located inside the inverse micelles, which assemble on a hexagonal lattice to form the H_{II}^C phase. This structure resembles that of the inverted hexagonal H_{II} phase of DOPE in excess water [31], with DNA replacing part of the water from the space inside the inverse micelles. Of note, not only the addition of lipid with negative spontaneous curvature, but also a strong reduction of the membrane bending rigidity κ by addition of cosurfactant (hexanol), can induce the shift from the lamellar (L_α^C) to the inverted hexagonal (H_{II}^C) phase of CL–DNA complexes [29].

The X-ray scattering pattern of the H_{II}^C phase clearly shows the q_{10}, q_{11}, q_{20}, and q_{21} reflections of the hexagonal lattice. The lattice spacing $a = 4\pi/(q_{10}\sqrt{3})$ was found to be consistent with the expected dimensions of DOTAP/DOPE monolayers and DNA with two hydration layers.

The recently discovered third, H_I^C CL–DNA phase [19] is also driven by the curvature. Just as the cone shape of DOPE favors a negative curvature of the lipid membrane because of its small head-group, lipids with a very large head-group (i.e., an inverted cone molecular shape) favor a positive curvature. Interestingly cationic lipids with up to five charges assemble into lamellar DNA complexes, even though some of them form spherical or cylindrical micelles in aqueous solution (without DNA). However, a recently synthesized lipid with 16 positive charges in the head-group (MVLBG2, see Table 16.1) exhibits the hexagonal H_I^C phase over a narrow range of composition around 25 mol% cationic lipid/75 mol% DOPC [19]. Other nonlamellar phases with, as of now, an undetermined structure are observed at higher contents of this highly charged lipid. The X-ray scattering pattern again shows peaks indicative of a hexagonal structure with the q_{10}, q_{11}, q_{20}, q_{21}, and q_{30} reflections visible. However, the lattice spacing a is increased to 81.5 Å (compared to 67.4 Å in the H_{II}^C phase), and this is due to the completely different arrangement of the lipid and DNA. In the H_I^C phase, cylindrical lipid micelles are arranged on a hexagonal lattice, and the DNA forms a honeycomb lattice in the interstices of this lipid arrangement.

The nanoscopic structure of CL–DNA complexes has a profound influence on their transfection mechanism. This effect will be discussed below, after introducing the two main compositional parameters that also affect vector performance.

16.3 EFFECT OF THE LIPID–DNA CHARGE RATIO (ρ_{chg}) ON CL–DNA COMPLEX PROPERTIES

One of the key parameters governing the properties and transfection efficiency of CL–DNA complexes is the ratio of lipid to DNA. While frequently the weight ratio of the total lipid or cationic lipid to DNA is reported, the most meaningful parameter is the cationic lipid– DNA charge ratio, ρ_{chg}. This is because complexes show universal or at least analogous physicochemical and biological behavior as a function of this parameter.

16.3.1 Physicochemical Effects and Phase Behavior of CL–DNA Lipids

At the isoelectric point, essentially all lipid and DNA are incorporated into the complex, which is without charge because the charges on lipid and DNA exactly compensate each other. Importantly there is a range of ρ_{chg} around the isoelectric point ($\rho_{chg} = 1$) where excess lipid (if $\rho_{chg} > 1$) or excess DNA (if $\rho_{chg} < 1$) is fully incorporated into the complexes, even though there no longer is an exact matching of charges. We refer to this phenomenon as "overcharging," because of the resulting excess charge in the complex either due to the lipid or the DNA. The corresponding excess counterions are not released into solution but still gain entropy: upon addition of excess DNA to an isoelectric complex, the counterions of that DNA are released into the "counterion vacuum" of the isoelectric complex and thus gain entropy. In other

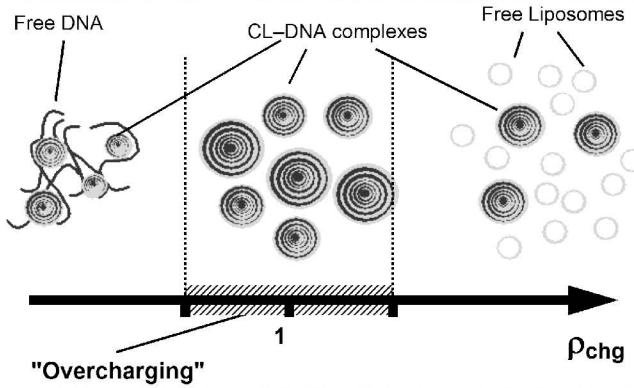

Figure 16.3 Schematic depiction of the regimes of CL–DNA complexes as a function of the lipid–DNA charge ratio ρ_{chg}. Around the isoelectric point, overcharging occurs as excess lipid or DNA is incorporated into the complexes. Beyond the limits of overcharging, phase separation sets in and CL–DNA complexes coexist with DNA ($\rho_{chg} < 1$) or liposomes ($\rho_{chg} > 1$) in solution.

words, incorporation of excess DNA into an isoelectric complex is driven by an osmotic concentration gradient between counterions near the DNA and inside the isoelectric complex. The incorporation of excess liposomes can be explained in a similar manner. Beyond a critical level of overcharging, additional charged species are no longer incorporated, and overcharged complexes coexist with free DNA or free liposomes in solution [28]. Figure 16.3 schematically shows the overcharging (single phase) and coexistence regimes as a function of ρ_{chg}.

The overcharging regime is not necessarily symmetrical around the isoelectric point. It is strongly influenced by the membrane charge density of the lipid membranes as well as by the solution conditions, in particular, the salt concentration. This is shown in Figure 16.4 (top), which shows a plot of the measured average DNA interaxial distances d_{DNA} for DOTAP/DOPC–DNA complexes of varied charge density in water and 150 mM NaCl solution. At the isoelectric point of L_α^C CL–DNA complexes, d_{DNA} is directly related to the lipid membrane charge density (σ_M): $d_{DNA} = e/(l_0\sigma_M)$, with l_0 designating the average distance per anionic charge along the DNA backbone [27,28]. For simple geometric reasons, d_{DNA} increases or decreases, respectively, as additional lipid or DNA is incorporated into the isoelectric complex. Thus d_{DNA} is a useful indicator of overcharging. All data in Figure 16.4 follow sigmoidal curves, consistent with the schematic picture shown in Figure 16.3. At the lowest charge ratios, d_{DNA} is shortest and constant until it starts to increase close to the isoelectric point. Note that in the figure, d_{DNA} is plotted against the DOTAP/DNA weight ratio ρ, with $\rho = 2.2 \times \rho_{chg}$. As seen in Figure 16.4, d_{DNA} increases through the isoelectric point until it saturates, marking the end of the overcharging regime. As expected from the model for overcharging described above, the overcharging regime extends over a wider range of ρ_{chg} as the membrane charge density of the lipid increases, namely, as the weight fraction neutral lipid (Φ_{DOPC}) decreases (Figure 16.4, top left) [28]. This is because the

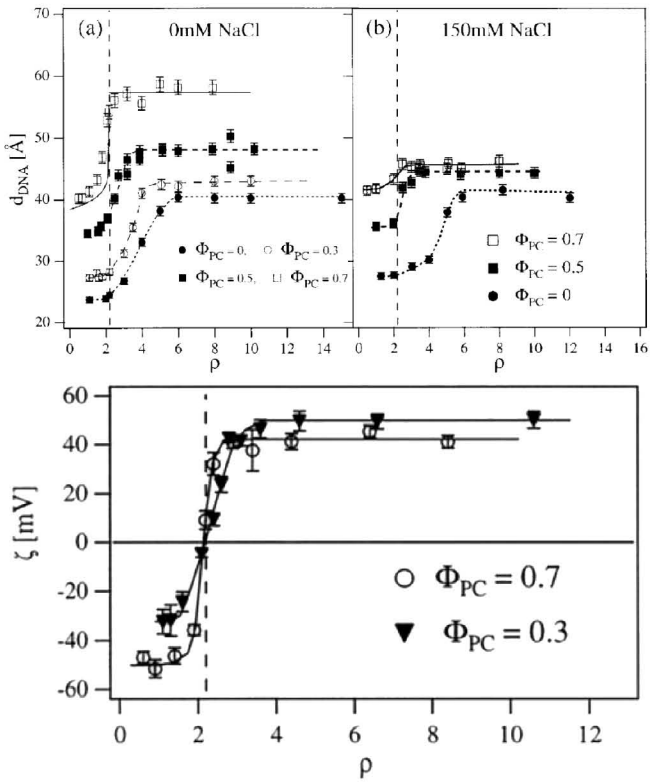

Figure 16.4 (*a*) Variation of the interhelical distance d_{DNA} with the DOTAP/DNA weight ratio $\rho = 2.2 \times \rho_{chg}$ in DOTAP/DOPC–DNA complexes with a fixed DOPC weight ratio Φ_{PC} and no salt. The vertical dashed line indicates the isoelectric point ($\rho = 2.2$). The solid line through the data at $\Phi_{PC} = 0.7$ is the result of nonlinear Poisson–Boltzman theory for complexes with low membrane charge density [24]. The dashed lines are guides to the eye. The complexes are single phase in the region of increasing d_{DNA}, coexisting with DNA at lower ρ and with lipid at higher ρ. (*b*) Same as (*a*) at 150 mM NaCl. All lines are guides to the eye. (*bottom*) Variation of the complex ζ-potential with changing ρ. The vertical line marks the isoelectric point ($\rho = 2.2$). Lines through the data are guides to the eye. (Reprinted with permission from [28]. © 1999 Biophysical Society)

confinement of the counterions increases with σ_M. Also in accordance with the model, complexes with lower σ_M incorporate more DNA (corresponding to an earlier onset of the increase in d_{DNA}). Apart from the increasing counterion concentration within the complex, the electrostatic repulsion between the additional DNA rods limits the amount of DNA that will be incorporated. The lower σ_M corresponds to a larger initial d_{DNA}, and thus less strong repulsion between the DNA rods.

The driving force of the counterion release mechanism is reduced by added salt. This is particularly true for counterion release from the lipid membrane, which relies

on a concentration gradient between the layer of ions confined close to the lipid membrane and the bulk solution. Since the Gouy–Chapman length scales with $1/\sigma_M$, the concentration of counterions next to the lipid membrane scales with σ_M. Therefore the addition of salt to a solution in which the complexes are formed has a stronger effect on complexes with low σ_M (high Φ_{DOPC}), as shown in Figure 16.4 (top right) for a NaCl concentration (150 mM) comparable to that of the cell culture media.

The results obtained by X-ray scattering and analysis of the DNA interaxial distances were corroborated by measurements of the zeta potential of CL–DNA complexes. As demonstrated by the typical data shown in Figure 16.4 (bottom), the zeta potential measurements also clearly demonstrate the effect of overcharging. Inversion of the surface potential consistently occurs at the isoelectric point. Of note, high σ_M complexes reach higher positive saturation zeta potentials, while low σ_M complexes display larger values of the negative saturation zeta potential. This effect is consistent with the complexes' ability to incorporate larger amounts of cationic lipid or DNA, respectively, as outlined above.

16.3.2 Biological Effects

The lipid–DNA charge ratio has a strong effect on the biological properties of CL–DNA complexes, as summarized in Figure 16.5. Figure 16.5 (top) exemplarily shows the effect of ρ_{chg} on the transfection efficiency as measured with a luciferase assay [20]. As was initially observed for DOTAP [32], the TE of all lipids studied in our group to date increases with ρ_{chg} up to a saturation value; this behavior is independent of the composition of the membrane. However, the charge ratio at which saturation occurs (ρ^*_{chg}) can vary among different families of lipids. This is seen in Figure 16.5 (top), which shows the transfection efficiencies of complexes with 60 mol% cationic lipid for DOTAP and the multivalent, dendritic lipids MVLG2, MVLBG1, and MVLBG2 (Table 16.1) [20] at various values of ρ_{chg}: a lipid–DNA charge ratio of 3 lies in the saturated regime for DOTAP, while the dendritic lipids require at least $\rho_{chg} = 4.5$. The start of the increase in the TE with ρ_{chg} for DOTAP is around the isoelectric point, which suggests a correlation with the surface charge. The exterior cell membrane contains many negatively charged polysaccharides, which have been implicated in the attachment and uptake of the CL–DNA complexes [33–35]. A cationic surface charge would thus favor attachment and internalization of the complex. However, zeta potential measurements have shown that the surface charge of DNA complexes of the dendritic lipids also changes sign at the isoelectric point (Figure 16.6). In addition a variation in the onset of efficient transfection with ρ_{chg} was observed between different cell lines [19]. Further work is necessary to fully understand how the lipid structure or its properties affect ρ^*_{chg}, with the goal of establishing rules to predict it.

Large amounts of cationic lipids or polymers are toxic to cells, with polymers typically being much more toxic than lipids on a "per charge" basis. Figure 16.5 (bottom) shows cell toxicities for complexes with 60 mol% DOTAP, MVLG2, MVLBG1, and MVLBG2 as a function of ρ_{chg}.Toxicities were measured using a commercially available assay that probes cell membrane integrity [20]. Note the

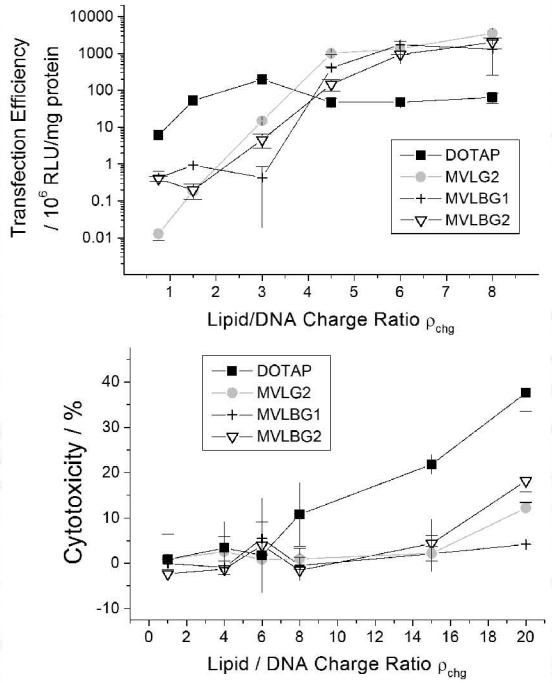

Figure 16.5 Transfection efficiency (*top*) and cytotoxicity (*bottom*) of DNA complexes containing 60 mol% cationic lipid at various lipid–DNA charge ratios. Note the difference in the scale of the charge ratio axes. The amount of DNA is constant for all data points. Transfection efficiencies were measured using a luciferase assay. Cytotoxicity was assessed with an assay that probes cell membrane integrity. (Reprinted with permission from [20].© 2006 American Chemical Society)

different scale of the ρ_{chg}-axis compared with the transfection efficiency plot. For all lipids in this plot, and all other lipids investigated in our laboratory, only the charge ratios much exceeding those required for efficient transfection produced any notable toxicity. Nevertheless, it is worth noting that the onset of the curve is much delayed for the dendritic lipids in comparison with DOTAP, demonstrating their reduced cytotoxicity. This may be important in newly emerging applications such as the delivery of small interfering RNA (siRNA) for gene silencing [36,37], which requires much higher values of ρ_{chg} than DNA delivery [38].

16.4 EFFECT OF THE MEMBRANE CHARGE DENSITY (σ_M) ON CL–DNA COMPLEX PROPERTIES

The second main compositional parameter of CL–DNA complexes is the ratio of neutral to cationic lipid. For comparative discussions, it is helpful to use the lipid

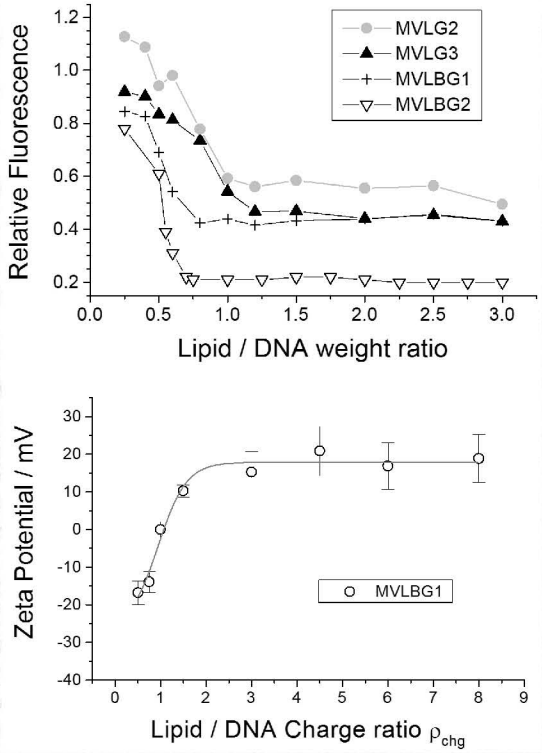

Figure 16.6 Data from an ethidium bromide (EtBr) displacement assay (*top*) used to measure the charge of dendritic multivalent lipids in complexes with DNA. EtBr fluoresces when intercalated into DNA but is expelled by lipid–DNA complex formation, which results in reduced fluorescence intensity due to self-quenching of EtBr in solution. The fluorescence intensity is normalized to that of DNA with EtBr and no lipid and plotted against the lipid/DNA weight ratio to resolve the data for the different lipids. Zeta potential of MVLBG1–DNA complexes (*bottom*) as a function of calculated ρ_{chg}. Analysis of the data from the EtBr displacement assay yielded Z_{exp}, which was used to calculate ρ_{chg}. The line (sigmoidal fit) is a guide to the eye. Note that the zeta potential changes sign at approximately $\rho_{chg} = 1$. (Adapted with permission from [20].© 2006 American Chemical Society)

membrane charge density, σ_M, to quantify this parameter. The membrane charge density is defined as the cationic charge per unit area. It may be thought of as a lipid-independent measure of how cationic a membrane is. For example, two membranes, each containing the same molar fraction of a cationic lipid, may exhibit very different values of σ_M if the two cationic lipids carry a different charge (provided that their head-group areas are the same). At the same time σ_M of two membranes containing very different molar fractions of cationic lipid may be similar if the two cationic lipids have very different charges. To calculate σ_M, one needs to know the charge of the cationic

lipid effective in DNA complexation and its head-group area:

$$\sigma_M = \frac{eZN_{cl}}{A_{nl}+A_{cl}} = \frac{1-\Phi_{nl}}{\Phi_{nl}+r\Phi_{cl}}\sigma_{cl},$$

where $r = A_{cl}/A_{nl}$ is the ratio of the head-group area of the cationic to neutral lipid, $\sigma_{cl} = eZ/A_{cl}$ is the charge density of the cationic lipid with valence Z, and $\Phi_{nl} = N_{nl}/(N_{nl}+N_{cl})$ and $\Phi_{cl} = N_{cl}/(N_{nl}+N_{cl})$ are the molar fractions of the neutral and cationic lipids, respectively.

The charge of the lipid can be determined using zeta potential measurements. An alternative and experimentally much simpler method is the ethidium bromide (EtBr) displacement assay. EtBr fluoresces when intercalated between the bases of DNA but self-quenches in solution. As shown in Figure 16.6 (top), addition of the cationic lipid to a mixture of DNA and EtBr results in a drop of fluorescence as EtBr is expelled upon the complex's formation. Analysis of the sigmoidal curves yields the charge of the lipid [18]. Figure 16.6 (bottom) exemplarily shows that the charge determined with the EtBr assay agrees with that obtained from the zeta potential measurements. Note that in Figure 16.6 (top), the lipid to DNA weight ratio is used as the abscissa to resolve the data for various lipids, while the zeta potential is plotted against the charge ratio calculated using Z from the EtBr assay.

The importance of the membrane charge density for the overcharging and stability of CL–DNA complexes in a salt solution has already been discussed. In addition the membrane charge density is a universal parameter governing the transfection efficiency of lamellar complexes. Early data for commercially available lipids of varied charge such as DOTAP (1+), DMRIE (1+), and DOSPA (5+) showed that DOSPA-containing complexes remained highly transfectant at much larger mol fractions of DOPC, as large as 0.7. At this composition, TE for the univalent cationic lipids is nearly two orders of magnitude lower [30]. A more detailed investigation explored the effect of a broad range of charge densities on TE, using a newly synthesized set of multivalent lipids (MVL2–(T)MVL5; see Table 16.1) [17,18]. X-ray diffraction showed that these MVLs form lamellar (L_α^C) MVL/DOPC–DNA complexes.

The TE results for DNA complexes of several MVLs at various MVL/DOPC ratios are shown in Figure 16.7. Corresponding data for DOTAP (as a monovalent lipid and a control) are also plotted. The amount of DNA was kept constant for all data points. Figure 16.7*A* shows TE as a function of the mol fraction of the cationic lipid. All cationic lipids exhibited a maximum in the TE as a function of the lipid composition: at 65 mol% for MVL2, 70 mol% for MVL3, 50 mol% for MVL5, 55 mol% for TMVL5, and 90 mol% for DOTAP. Thus, while the optimized TE is similar for all lipids, this TE appeared at different molar ratios. This behaviour demonstrates the importance of optimizing the ratio of neutral to cationic lipid for novel cationic lipids. Such optimization should go beyond the testing of only a few integer ratios often seen in the literature. The optimal lipid compositions result in a TE that is about three orders of magnitude larger than that of complexes with poor efficiency.

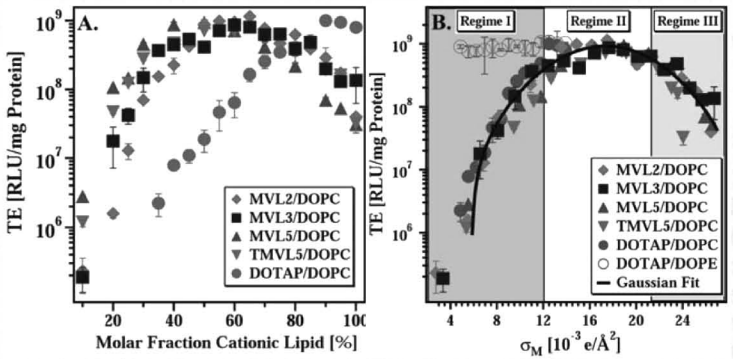

Figure 16.7 (*A*) Transfection efficiency (TE) as a function of the molar fraction cationic lipid for CL/DOPC–DNA complexes prepared with MVL2 (*diamonds*), MVL3 (*squares*), MVL5 (*triangles*), TMVL5 (*inverted-triangles*), and DOTAP (*circles*). All data was taken at $\rho_{chg} = 2.8$, using the same amount of DNA for each data point. (*B*) The same TE data plotted against the membrane charge density, σ_M. The solid line is a Gaussian fit to the data. Data for DOTAP/DOPE–DNA complexes (*open circles*, H_{II}^C phase) are also shown. Three regimes of transfection efficiency are labeled. Reproduced with permission from [18]. (Copyright 2005 John Wiley & Sons Limited.)

Figure 16.7*B* shows the same transfection efficiency data, now plotted against the membrane charge density, σ_M. Remarkably a notable simplification takes place, and all the data points merge onto a single curve. This demonstrates that σ_M is a universal parameter and a predictor of transfection efficiency for lamellar (L_α^C) CL–DNA complexes. The resulting universal curve reveals an optimal charge density of $\sigma_M^* = 17.0 \pm 0.1 \times 10^{-3}$ (e/Å^2) [18].

The universal curve for the TE of L_α^C complexes shown in Figure 16.7*B* displays three distinct regimes. In the low σ_M regime (regime I), TE increases exponentially with the membrane charge density: for small values of σ_M, a straight line fits the data well. In regime III, at very high σ_M, TE decreases exponentially with σ_M. Between these regimes there is a resulting regime of optimal TE, centered around σ_M (regime II). When transfection experiments are performed in the presence of chloroquine, a weak base that disrupts endosomes, only the TE of complexes in regime I is improved. This suggests that in regime I, endosomal escape is the limiting step in the transfection process [18,30]. Confocal microscopy experiments (see below) further support this finding. Escape from the endosome likely occurs via an activated fusion process of the oppositely charged membranes of endosome and complex [30]. The activation energy for this can be written as $\delta E = a\kappa - b\sigma_M$, where a and b are constants >0. The parameter κ is the bending rigidity of the membrane, which is mainly determined by the lipid tails and therefore constant in the described experiments. The bending of membranes, as required for fusion, results in an energy cost proportional to κ. Since the interacting membranes are oppositely charged, the activation energy decreases with increasing σ_M. If endosomal entrapment limits transfection as proposed earlier, the activation energy for fusion directly relates σ_M to the transfection efficiency via an

Arrhenius-type equation, predicting the observed exponential increase of TE with σ_M [30]:

$$\text{TE} \propto \text{Rate of fusion} = \frac{1}{\tau} e^{-\delta E/kT}.$$

Here $1/\tau$ is the collision rate between the trapped CL–DNA particle and the endosomal membrane.

16.5 EFFECT OF NONLAMELLAR CL–DNA COMPLEX STRUCTURE ON THE TRANSFECTION MECHANISM

Figure 16.7*B* also shows the TE data for DOTAP/DOPE–DNA complexes (hollow circles). The TE of these complexes does not follow the universal curve at small membrane charge densities (high content of neutral lipid), where they are in the inverted hexagonal (H_{II}^C) phase. This suggests that H_{II}^C and L_α^C complexes transfect by fundamentally different mechanisms, and that endosomal escape/fusion of the complex and endosomal membranes are not limiting the TE for H_{II}^C complexes (see also confocal microscopy results below). The highly charged head groups of the dendritic cationic lipids MVLBG1 (8+) and MVLBG2 (16+) give access to very high membrane charge densities. However, as shown in Figure 16.8, their TE does not decrease at high σ_M. While this does not match with the universal TE curve of Figure 16.7*B*, complexes of these dendritic lipids are no longer in the lamellar phase beyond 25 (MVLBG2) and 40 (MVLBG1) mol% cationic lipid. This further demonstrates the strong effect of the complex structure on the transfection pathways and suggests that the release of DNA from highly charged lipid membranes may be more facile for H_I^C than for L_α^C complexes.

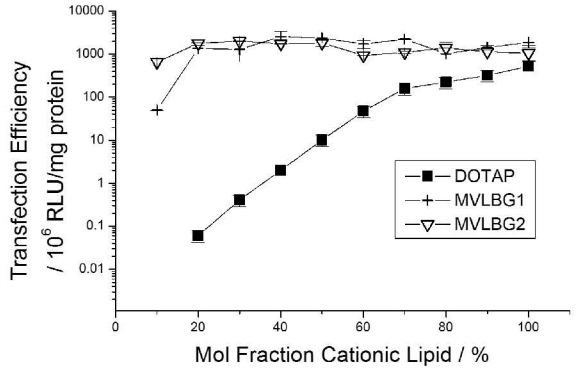

Figure 16.8 Transfection efficiency of DNA complexes of DOTAP, MVLBG1, and MVLBG2 plotted against the mol fraction of cationic lipid in mixtures with DOPC. All data points were taken at a lipid–DNA charge ratio of 6, using a constant amount of DNA. (Reprinted with permission from [20]. © 2006 American Chemical Society)

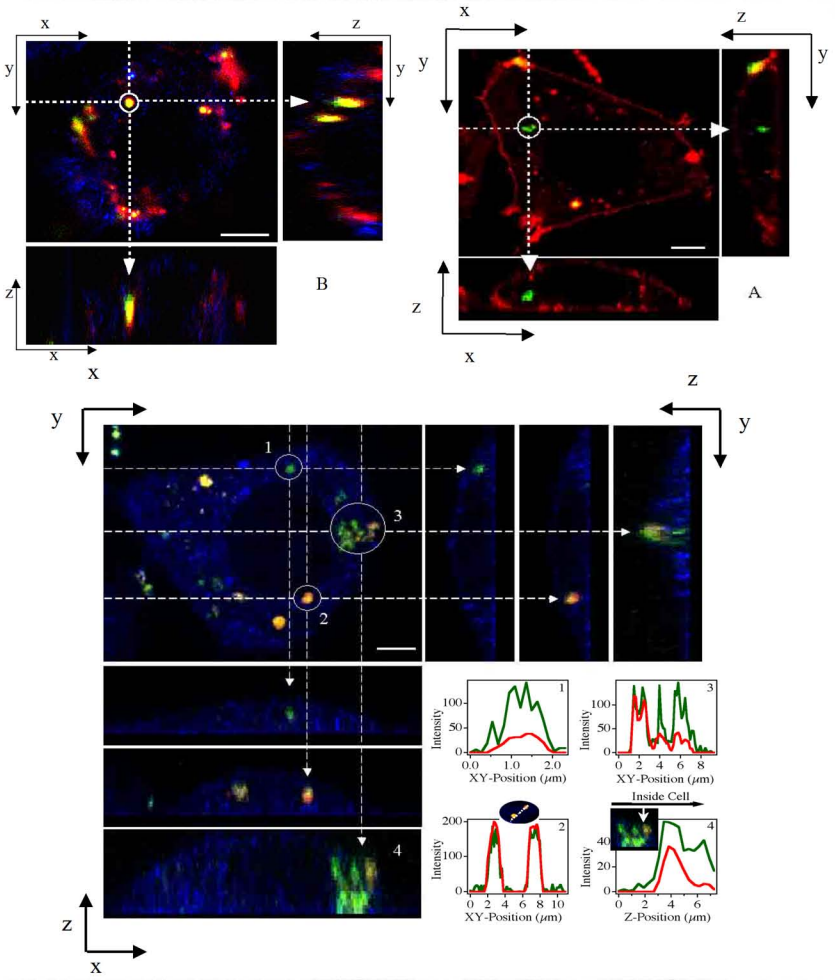

Figure 16.9 Laser scanning confocal microscopy images of transfected mouse L cells, fixed six hours after incubation with complexes. Red and green fluorescence corresponds to lipid and DNA labels, respectively; yellow, the overlap of the two, denotes CL–DNA complexes. The cell outline was observed in reflection mode, appearing in blue. Scale bars are 5 μm. For each set of images, middle is the *x*-*y* (*top*) view at a given *z*; right is the *y*-*z* side view along the vertical dotted line; bottom is the *x*-*z* side view along the horizontal dotted line. Arrows in the side views mark objects circled in the top view. (*Top left*) A cell transfected with L_{α}^{C} DOTAP/DOPC–DNA complexes at $M_{DOPC} = 0.67$ for which TE is low, as shown in Figure 16.7. No evidence for fusion is visible and only intact CL–DNA complexes such as the one marked by a circle are observed inside the cells. This observation implies that DNA remains trapped within the complexes, consistent with the observed low transfection efficiency. (*Top right*) Cells transfected with H_{II}^{C} DOTAP/DOPE–DNA complexes ($M_{DOPE} = 0.69$) show transfer of fluorescent lipid to the cell plasma membrane and the release of DNA (green; in the circle) within the cell. (*Bottom*) A typical LSCM image of a cell transfected with L_{α}^{C} complexes at $M_{DOPC} = 0.18$, corresponding to cationic membranes with a high charge density $\sigma_M \approx 0.012$ e/A^2 and high TE (see Figure 16.7). Although the lamellar complexes used here show high TE, no lipid transfer to the cell plasma membrane is seen in contrast to high-transfecting H_{II}^{C} complexes. Both released DNA (1) and intact complexes (2) are observed inside the cell. Labels (3) and (4) : A complex in the process of releasing its DNA into the cytoplasm. For objects labeled with numbers, plots of fluorescence intensity as a function of position are shown in boxes in the lower right corner. (Reprinted with permission from [30]. © 2003 Biophysical Society) (See color plate.)

It is important to note that optimized CL–DNA complexes, independent of their structure, transfect equally well in the in vitro conditions of our experiments (Figures 16.7 and 16.8). Thus far we have observed a notable difference in the performance between optimized complexes of different lipids in only one instance: the TE of complexes of MVLBG2 in a "hard to transfect" embryonic mouse fibroblast cell line was an order of magnitude higher than their DOTAP counterparts [19].

Laser scanning confocal microscopy (LSCM), which provides true three-dimensional imaging with micrometer resolution, has yielded further insight into the transfection pathways of lamellar and inverted hexagonal complexes. Figure 16.9 shows typical LSCM micrographs of cells fixed after six hours of incubation with H_{II}^{C} complexes as well as L_{α}^{C} complexes at high and low σ_M. Lipid and DNA were labeled using red and green fluorescent probes, respectively. Their overlap appears yellow, and the cell outline blue (reflection mode).

In the case of the H_{II}^{C} complexes (Figure 16.9, top right), the mixing of cellular and complex lipids is evident from the fluorescent labeling of the cell membrane. In addition free DNA is observed in the cytoplasm. The observed lipid mixing is indicative of fusion, either before or after endocytosis of the complexes. In stark contrast, only intact complexes and no lipid mixing are observed for low σ_M lamellar complexes (Figure 16.9, top left). The lack of indications for fusion suggests that complexes are taken up via endocytosis. No evidence for escape from the endosome nor dissociation of the complexes is seen. While high σ_M lamellar complexes (Figure 16.9, bottom) also do not show lipid mixing, both free DNA as well as a few intact complexes are visible inside the cell. Thus these complexes also enter via endocytosis, but they are able to release their DNA. Moreover, since the free DNA is in a condensed state but there are no DNA-condensing compounds in the endosome, the DNA must reside in the cytoplasm, which implies endosomal escape.

16.6 MODEL OF TRANSFECTION WITH LAMELLAR CL–DNA COMPLEXES

The results from diverse methods have provided keys to an extended understanding of the mechanism of transfection by lamellar CL–DNA complexes [18,30]. Figure 16.10 schematically depicts the features of this model.

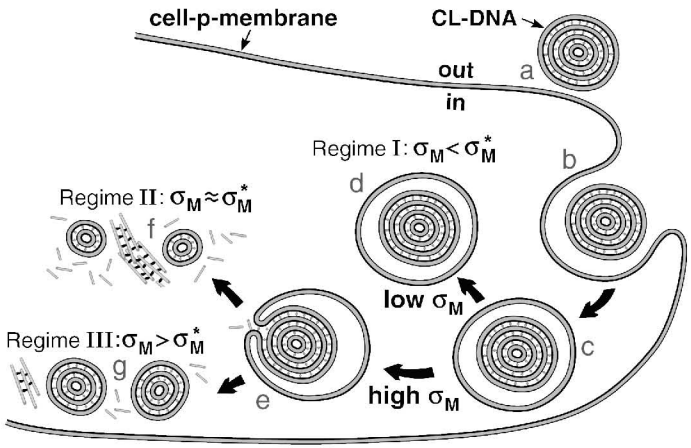

Figure 16.10 A model of the cellular pathway and transfection mechanism of L_α^C complexes. Cationic complexes adhere to cells due to favorable electrostatic interactions (*a*) and enter through endocytosis (*b* and *c*). Complexes with low σ_M largely remain trapped in endosomes (*d*). Complexes with high σ_M escape the endosome through activated fusion (*e*). The released smaller complexes dissociate more or less effectively by interactions with charged macromolecules inside the cell, depending on their σ_M (*f* and *g*). Strong membrane–DNA interactions at very high σ_M may lead to diminished dissociation (*g*), but efficient release occurs at $\sigma_M \approx \sigma_M^*$ (*f*). (Reproduced with permission from [18]. Copyright 2005 John Wiley & Sons Limited)

The initial attachment to the cell is mediated by electrostatics (Figure 16.10*a*) and followed by endocytosis (Figure 16.10*b*). The three regimes of the universal TE curve shown in Figure 16.7*B* correspond to distinct complex–cell interaction regimes occurring after endocytosis [18]. For complexes with low $\sigma_M < \sigma_M^*$ (regime I), endosomal escape limits the TE (Figure 16.10*c* and *d*). Some complexes escape via activated fusion with the endosomal membrane, resulting in the exponential increase of TE with σ_M over three orders of magnitude.

At higher σ_M (regimes II and III), the TE is no longer limited by endosomal escape, as demonstrated using a chloroquine assay and by confocal microscopy [18,30]. These complexes fuse easily with the endosomal membrane, releasing smaller complexes into the cytoplasm (Figure 16.10*e*). However, at very high $\sigma_M > \sigma_M^*$ (regime III), the TE *decreases* with σ_M. It is possible that transfection is limited by complex dissociation in the cytoplasm, which is due to the strong electrostatic interaction between the DNA and the highly charged lipid bilayers (Figure 16.10*g*). The optimal TE observed in regime II reflects a compromise between opposing requirements (Figure 16.10*f*): escape from the endosomes requires high σ_M, but dissociation of complexes in the cytoplasm requires low σ_M. Future strategies to optimize the TE of lamellar CL–DNA complexes must strive to decouple these opposing requirements. This is particularly important in view of the abundance of the lamellar structure and the fact that DOPE has turned out to be an undesirable lipid for in vivo applications.

16.7 MODEL OF TRANSFECTION WITH INVERTED HEXAGONAL CL–DNA COMPLEXES

As indicated by their deviation from the universal curve of Figure 16.7*B* and the extensive mixing of complex and cell membrane lipids observed by confocal microscopy (Figure 16.9), CL–DNA complexes in the inverted hexagonal phase are prone to membrane fusion. This is intimately related to their structure and the preferred curvature of lipid membranes containing DOPE [30]. As schematically shown in Figure 16.11, the outermost lipid monolayer, which must cover any H_{II}^C complex to provide a hydrophilic surface, exhibits a curvature opposite to that of the preferred (negative) curvature of the lipids coating DNA inside the complex. This elastically frustrated state of the outer monolayer, which is independent of σ_M, drives the rapid fusion with the plasma or endosomal membrane, leading to release of a layer of DNA

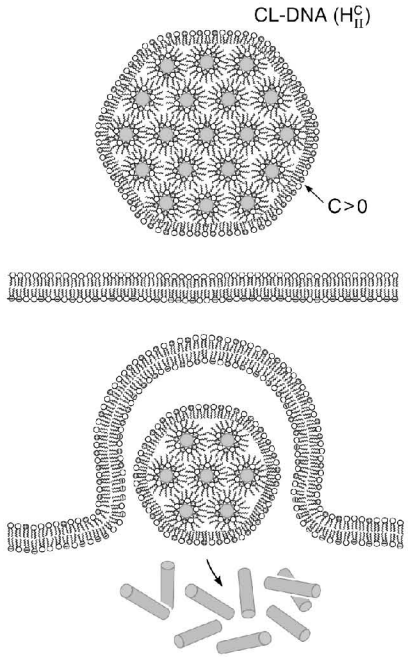

Figure 16.11 Schematic of an inverted hexagonal CL–DNA complex interacting with the plasma membrane or the endosomal membrane. The outer lipid monolayer covering the H_{II}^C complex has a positive curvature, whereas the preferred curvature of DOPE-containing membranes is negative, as realized in the monolayers coating DNA. Thus the outer layer is energetically costly. This results in a driving force, independent of the cationic membrane charge density, for rapid fusion of the H_{II}^C complex with the bilayer of the cell plasma membrane or the endosomal membrane. (Reprinted with permission from [30]. © 2003 Biophysical Society)

and a smaller H_{II}^{C} complex within the cell. The process can then repeat itself until all DNA is released from the complex. In contrast, the bilayer structure of lamellar L_{α}^{C} complexes is inherently more stable and release of DNA only occurs as the complex is disassembled, layer by layer, through interactions of the cationic membranes with anionic components of the cell such as the predominantly anionic actin and microtubule cytoskeletal filaments [39,40].

16.8 PEGYLATED CL–DNA COMPLEXES: SURFACE FUNCTIONALIZATION AND DISTINCT DNA–DNA INTERACTION REGIMES

Simple CL–DNA complexes as described above are successful for in vitro transfection of many mammalian cell lines and are currently used in ex vivo and in vivo clinical trials (e.g., involving intra-tumoral injection methods) [4,41]. However, they are not well suited for systemic applications. Both cationic lipids and their DNA complexes activate the complement system [42], which results in their rapid removal from circulation by the mononuclear phagocytic system cells through opsonization. As previously established for liposomes [43–46], conjugation of poly(ethyleneglycol) (PEG) to nonviral vectors can reduce the activation of the complement system [42]. The presence of a hydrophilic polymer shell provides a repulsive barrier and results in vastly increased circulation lifetimes, a phenomenon referred to as steric stabilization. Thus incorporating PEG-lipids is an essential step in making CL–DNA complexes viable for systemic gene delivery. In future applications functionalized PEG-lipids of variable length may also be used to add functionality and specificity to CL–DNA complexes by acting as tethers for target-specific ligands (e.g., peptides). Thus it is crucial to gain an understanding of the effects of incorporating PEG-lipids into CL–DNA complexes.

16.8.1 DNA–DNA Interaction Regimes in PEG-Lipid CL–DNA Complexes

Recent work has probed the structure, morphology, and function of CL–DNA complexes containing a ternary mixture of DOTAP, DOPC, and PEG-lipids [16,47]. It was shown that a critical value of PEG chain length exists, above which steric stabilization and other polymer-specific effects become evident. The structures of the investigated lipids are displayed in Figure 16.1. X-ray diffraction of isoelectric ($\rho_{chg} = 1$) complexes revealed a single phase of stable lamellar complexes for the PEG400-lipids. The lamellar structure was also observed for the PEG2000-lipids, but phase separation occurs at higher contents of the PEG-lipid (>7 mol% for PEG2000^{2+}-lipid; >10 mol% for PEG2000-lipid). Complete incorporation of added PEG-lipid into the complexes is not possible beyond these limits. Three distinct DNA interchain interaction regimes exist as a function of composition, due to (1) long-range repulsive electrostatic forces, (2) short-range repulsive hydration forces, and (3) a novel polymer-induced attractive depletion force in two dimensions.

The effect of incorporating PEG400^{2+}-lipid into isoelectric CL–DNA complexes was studied by monitoring the average interaxial distance between DNA chains (d_{DNA}; see Figure 16.2) while increasing the mol fraction of PEG400^{2+}-lipid at various constant mol fractions of DOTAP (M_{DOTAP}). The results reveal that PEG400^{2+}-lipid simply acts as an additional cationic lipid, leading to the condensation of DNA through an increase in the membrane charge density. As with DOTAP [48], two distinct DNA interaction regimes are observed. In the electrostatic regime (4×10^{-3} e/Å^2 < σ_M < 8.5×10^{-3} e/Å^2), d_{DNA} depends purely on the membrane charge density. In the regime of $\sigma_M > 8.5 \times 10^{-3}$ e/Å^2, a strong repulsive hydration barrier between DNA rods dominates [48], preventing further condensation of the DNA. Neutral PEG400-lipid also shows no polymer-specific behavior, presumably because of the short chain length ($<n> = 9$): its exchange with DOPC does not affect the DNA spacing.

A distinctly different picture arises for PEG-lipids with chains of molecular weight 2000 g/mol ($<n> = 45$). Figure 16.12 (left) shows XRD data from single-phase DOTAP/DOPC–DNA complexes of constant $M_{DOTAP} = 30\%$ containing increasing amounts of neutral PEG2000-lipid. The DNA interaxial spacing ($d_{DNA} = 2\pi/q_{DNA}$) decreases from 53.7 Å (without PEG-lipid) to 49.1 Å (1.6 mol% PEG-lipid) to 41.6 Å (6.7 mol% PEG-lipid) with increasing mole fraction of the PEG2000-lipid, indicating the existence of an additional attractive force. This force is due to the presence of a polymer chain in the confined space between the lipid bilayers where the DNA chains reside (depletion attraction force; see below). The fact that addition of neutral as well as cationic (data not shown) PEG2000-lipid decreases the DNA spacing confirms that the polymer chain–DNA interaction is the dominating effect of adding PEG2000-lipids, as opposed to electrostatics in the case of PEG400-lipids. For complexes with $\sigma_M > 8 \times 10^{-3}$ e/Å^2, the repulsive hydration forces again dominate the interactions between the DNA rods [47].

Figure 16.12*A* schematically shows the origin of the polymer-induced depletion attraction force between DNA strands. This phenomenon is well known in bulk solution, but much larger PEG molecular weights are required in three dimensions [49]. PEG of molecular weight 2000 Da has a radius of gyration of roughly 35 Å [50,51]. Thus the PEG2000 part of the PEG2000-lipid will be excluded from regions between DNA rods [52], for which the electrostatically calculated values of d_{DNA} dictate a width of 5 to 35 Å. This causes a phase separation between the polymer and the DNA within the layers of the complex, as shown schematically in Figure 16.12*B* and *C*. The decreased DNA spacing then is a result of osmotic stress exerted on the DNA domains by the PEG2000 chains confined to the outside of these domains, which increases with the concentration of polymer. As depicted in Figure 16.12*B* and *C*, the resulting complex has DNA-rich domains, shown in dark gray, and polymer-rich domains, shown in light gray.

16.8.2 Surface Functionalization of CL–DNA Complexes with PEG-Lipids

Optical microscopy of PEG-lipid/CL–DNA complexes at $\rho_{chg} = 2.8$ and M_{DOTAP} 0.82 in a cell culture medium (DMEM) was performed to demonstrate surface

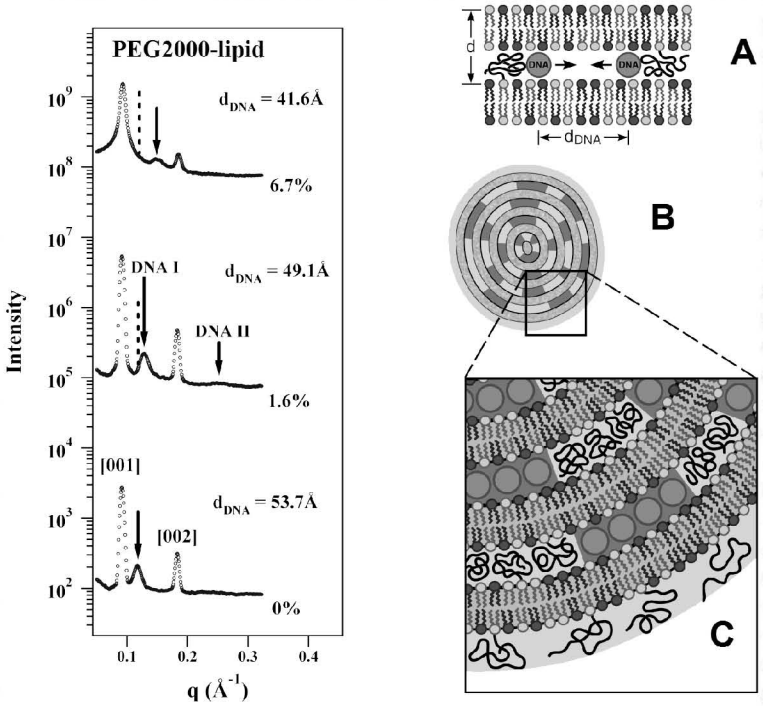

Figure 16.12 (*Left*) XRD scans of L_{α}^{C} DOTAP/DOPC–DNA complexes containing varied amounts of PEG2000-lipid. Arrows mark the DNA interhelical peaks, which move to larger q_{DNA} (corresponding to a decrease of d_{DNA}) as PEG2000-lipid is added to the membranes of the complex. The dashed lines mark the position of q_{DNA} for 0% PEG-lipid. (*Right*) Schematics of a lamellar CL–DNA complex containing long-chain PEG-lipids. *(A)* A depletion attraction force cause by the presence of the polymer packs the DNA rods closer than predicted by electrostatics. *(B)* Cross section of a PEG-lipid/CL–DNA complex with DNA-rich domains (dark gray) and polymer-rich domains (light gray) in between lipid bilayers (gray). *(C)* Enlarged view showing the internal phase separation as well as the outer shell of polymer chains. (Reprinted in part with permission from [47]. © 2004 Biophysical Society)

coverage by the PEG-lipids and further pinpoint their distinct, chain length dependent behavior [47]. Figure 16.13*A* shows complexes without any PEG-lipid. Some aggregation is observed, because of the presence of salts in DMEM. Figure 16.13*B* shows complexes at $M_{PEG400\text{-}lipid} = 10\%$. Again, aggregation is clearly evident. However, complexes prepared using the long-chain PEG-lipid at $M_{PEG2000\text{-}lipid} = 10\%$ demonstrate a strong shielding effect of the polymer (Figure 16.13*C*). No aggregation of complex particles occurs, because of the steric repulsion conferred by the shell of the PEG2000-lipid polymer chains. As was mentioned earlier, this steric stabilization is important for developing a viable in vivo gene delivery system [53–55].

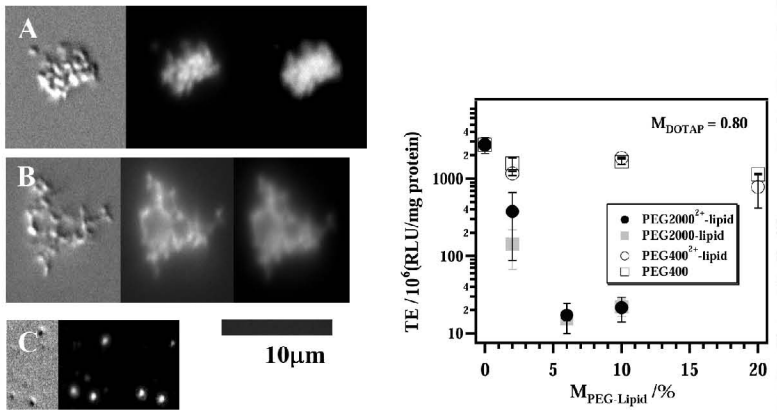

Figure 16.13 (*Left*) Microscopy images of DOTAP/DOPC–DNA complexes a $M_{DOTAP} = 0.33$ in the presence of cell culture medium (DMEM), taken in DIC (*left*), lipid fluorescence (*center*), and DNA fluorescence modes. The images show complexes prepared (*A*) without PEG-lipid (*B*), with 10 mol% PEG400-lipid, and (*C*) with 10 mol% PEG2000-lipid. The complex particles aggregate when no PEG-lipid or PEG400-lipid are added but are sterically stabilized by 10 mol% PEG2000-lipid. (*Right*) Transfection efficiency of PEG-lipid/DOTAP/DOPC–DNA complexes as a function of increasing molar fraction of PEG-lipid ($M_{PEG\text{-}lipid}$), at constant $M_{DOTAP} = 0.80$. Addition of PEG2000^{2+}-lipid or PEG2000-lipid reduces TE by nearly two orders of magnitude with only 6 mol% added PEG-lipid. By contrast, adding PEG400^{2+}-lipid or PEG400-lipid does not change TE significantly, even at 20 mol% PEG-lipid. As a reference, TE for naked DNA is typically on the order of 0.3×10^6 RLU/mg protein. Note that 20 mol% PEG400-lipid and 6 mol % PEG2000-lipid correspond to an approximately equal total weight of PEG. (Reprinted with permission from [47]. © 2004 Biophysical Society)

Figure 16.13 (right) shows transfection results for positively charged, PEG-lipid containing CL–DNA complexes ($\rho_{chg} = 2.8$) [47]. At $M_{DOTAP} = 0.80$, the transfection efficiency is high without added PEG-lipid, but the addition of 6 mol% PEG2000-lipid or PEG2000^{2+}-lipid abolishes most of this activity, reducing TE by about 2 orders of magnitude. This suggests that electrostatic binding of the cationic CL–DNA complexes to cells is strongly reduced by the shielding of the complex by the PEG2000 polymer layer with a thickness roughly equivalent to 35 Å. In contrast, the addition of a cationic or a neutral PEG400-lipid only negligibly affects the TE, even at 20 mol% PEG400-lipid. As suggested by the microscopy images, no shielding occurs with these shorter amphiphiles. At the same time the further addition of cationic lipid (PEG400^{2+}) does not improve transfection in this regime of high σ_M where the TE is at a maximum (Figure 16.7). Note that 6 and 20 mol% of the PEG2000-lipid and the PEG400-lipid, respectively, correspond to an approximately equal total weight of PEG.

In summary, microscopy and transfection experiments show that the added PEG-lipid coats the surfaces of the complexes, whereas X-ray diffraction results reveal that

the PEG-lipid is located internally as well. The next step on the way to CL–DNA complexes for in vivo applications will be to recover the potential for cell adhesion, for instance, by attaching specific, adhesion-mediating peptides to the distal end of some of the PEG chains.

16.9 CONCLUSION AND SUMMARY

The immense promise that gene therapy holds for future medical applications is reflected by a large amount of basic, applied, and clinical research in this field. Complexes of cationic lipids and DNA, as one of the most prominent examples of nonviral vectors for gene delivery/gene therapy, will be preferable over viral vectors if their limited transfection efficiency can be improved. To this end it is important to gain an understanding of the transfection mechanisms of CL–DNA complexes and the parameters governing their efficiency. Recent work reviewed in this chapter has shown how the CL–DNA complex structure, the lipid/DNA charge ratio (ρ_{chg}), and the membrane charge density (σ_M) affect the transfection efficiency (TE), while also providing insight into the distinct delivery mechanisms on a molecular level.

The molecular shape of the lipids determines the complex structure, which in turn determines the transfection mechanism. Three phases of CL–DNA complexes have been characterized and their structures determined so far: the lamellar (L_α^C), the inverted hexagonal (H_{II}^C), and the hexagonal (H_I^C) phase. The lamellar structure is the most abundant of these. For a given structure and thus transfection mechanism, ρ_{chg} and σ_M are key parameters affecting the transfection efficiency. In particular, σ_M is a universal parameter governing TE of lamellar complexes. Three distinct regimes of the TE as a function of σ_M exist, corresponding to different complex–cell interactions. The regime of the highest TE is found at intermediate membrane charge density, indicating and emphasizing the importance of optimizing the neutral/cationic lipid ratio, especially for multivalent lipids.

ACKNOWLEDGMENTS

We gratefully acknowledge useful discussions with A. Ahmad, N. F. Bouxsein, H. M. Evans, A. Martin-Herranz, A. J. Lin, N. Slack, A. Zidovska, and C. X. George. The reported work was supported by grants GM-59288, AI-12520, and AI-20611 from the National Institutes of Health of the United States. Support for the structure studies was also provided by the National Science Foundation DMR 0503347. The synchrotron X-ray diffraction experiments were carried out at the Stanford Synchrotron Radiation Laboratory, which is supported by the US Department of Energy. This work made use of MRL Central Facilities supported by the MRSEC Program of the National Science Foundation under award No. DMR05-20415.

REFERENCES

[1] P. L. Felgner, T. R. Gader, M. Holm, R. Roman, H. W. Chan, M. Wenz, J. P. Northrop, G. M. Ringold, M. Danielsen. Lipofection: A highly efficient, lipid-mediated DNA-transfection procedure. *Proc. Natl. Acad. Sci. USA* 84 (1987): 7413–7417.

[2] L. Huang, M. -C. Hung, E. Wagner (Eds.). *Advances in Genetics: Non-Viral Vectors for Gene Therapy*, Vol. 53 2 ed., Elsevier, San Diego, 2005.

[3] L. Huang, M. -C. Hung, E. Wagner (Eds.). *Nonviral Vectors for Gene Therapy*. Academic Press, San Diego, 1999.

[4] R. I. Mahato, S. W. Kim (Eds.). *Pharmaceutical Perspectives of Nucleic Acid-Based Therapeutics*. Taylor and Francis, London, 2002.

[5] For a recent set of reviews, see *Curr. Med. Chem.* 11 (2004): 133–220 and *Curr. Med. Chem.* 10 (2003): 1185–1315.

[6] T. Niidome, L. Huang. Gene therapy progress and prospects: Nonviral vectors. *Gene Ther.* 9 (2002): 1647–1652.

[7] A. D. Miller. Cationic liposomes for gene therapy. *Angew. Chem., Int. Ed.* 37 (1998): 1768–1785.

[8] Extensive and current information on clinical trials in the field of gene therapy is available at *http://www.wiley.co.uk/genetherapy/clinical/* (site of *J. Gene Med. Clin. Trial*, 2006).

[9] M. L. Edelstein, M. R. Abedi, J. Wixon, R. M. Edelstein. Gene therapy clinical trials worldwide 1989–2004—An overview. *J. Gene Med.* 6 (2004): 597–602.

[10] M. Cavazzana-Calvo, S. Hacein-Bey, G. de Saint Basile, F. Gross, E. Yvon, P. Nusbaum, F. Selz, C. Hue, S. Certain, J. -L. Casanova, P. Bousso, F. Le Deist, A. Fischer. Gene therapy of human severe combined immunodeficiency (SCID)-X1 disease. *Science* 288 (2000): 669–672.

[11] S. E. Raper, N. Chirmule, F. S. Lee, N. A. Wivel, A. Bagg, G. -P. Gao, J. M. Wilson, M. L. Batshaw. Fatal systemic inflammatory response syndrome in a ornithine transcarbamylase deficient patient following adenoviral gene transfer. *Mol. Genet. Metab.* 80 (2003): 148–158.

[12] S. Hacein-Bey-Abina, C. von Kalle, M. Schmidt, F. Le Deist N. Wulffraat, E. McIntyre, I. Radford, J. -L. Villeval, C. C. Fraser, M. Cavazzana-Calvo, A. Fischer. A serious adverse event after successful gene therapy for X-linked severe combined immunodeficiency. *N. Engl. J. Med.* 348 (2003): 255–256.

[13] S. Hacein-Bey-Abina, C. Von Kalle M. Schmidt, M. P. McCormack, N. Wulffraat, P. Leboulch, A. Lim, C. S. Osborne, R. Pawliuk, E. Morillon, R. Sorensen, A. Forster, P. Fraser, J. I. Cohen, G. de Saint Basile I. Alexander, U. Wintergerst, T. Frebourg, A. Aurias, D. Stoppa-Lyonnet, S. Romana, I. Radford-Weiss, F. Gross, F. Valensi, E. Delabesse, E. Macintyre, F. Sigaux, J. Soulier, L. E. Leiva, M. Wissler, C. Prinz, T. H. Rabbitts, F. Le Deist A. Fischer, M. Cavazzana-Calvo. LMO2-associated clonal T cell proliferation in two patients after gene therapy for SCID-X1. *Science* 302 (2003): 415–419.

[14] J. O. Rädler, I. Koltover, T. Salditt, C. R. Safinya. Structure of DNA–cationic liposome complexes: DNA intercalation in multilamellar membranes in distinct interhelical packing regimes. *Science* 275 (1997): 810–814.

[15] J. J. Harrington, G. van Bokkelen R. W. Mays, K. Gustashaw, H. F. Willard. Formation of de novo centromeres and construction of first-generation human artificial microchromosomes. *Nat. Genet.* 15 (1997): 345–355.

[16] U. Schulze, H. -W. Schmidt, C. R. Safinya. Synthesis of novel cationic poly(ethyleneglycol) containing lipids. *Bioconjugate Chem.* 10 (1999): 548–552.

[17] K. Ewert, A. Ahmad, H. M. Evans, H. -W. Schmidt, C. R. Safinya. Efficient synthesis and cell-transfection properties of a new multivalent cationic lipid for nonviral gene delivery. *J. Med. Chem.* 45 (2002): 5023–5029.

[18] A. Ahmad, H. M. Evans, K. Ewert, C. X. George, C. E. Samuel, C. R. Safinya. New multivalent lipids reveal bell curve for transfection efficiency versus membrane charge density: Lipid–DNA complexes for gene delivery. *J. Gene Med.* 7 (2005): 739–748.

[19] K. K. Ewert, H. M. Evans, A. Zidovska, N. F. Bouxsein, A. Ahmad, C. R. Safinya. A columnar phase of dendritic lipid-based cationic liposome–DNA complexes for gene delivery: Hexagonally ordered cylindrical micelles embedded in a DNA honeycomb lattice. *J. Am. Chem. Soc.* 128 (2006): 3998–4006.

[20] K. K. Ewert, H. M. Evans, N. F. Bouxsein, C. R. Safinya. Dendritic cationic lipids with highly charged headgroups for efficient gene delivery. *Bioconjugate Chem.* 17 (2006): 877–888.

[21] G. S. Manning. Limiting laws and counterion condensation in polyelectrolyte solutions. I. Colligative properties. *J. Chem. Phys.* 51 (1978): 924–933.

[22] M. Le Bret B. H. Zimm. Distribution of counterions around a cylindrical polyelectrolyte and Manning's condensation theory. *Biopolymers* 23 (1984): 287–312.

[23] D. Harries, S. May, W. M. Gelbart, A. Ben-Shaul. Structure, stability, and thermodynamics of lamellar DNA-lipid complexes. *Biophys. J.* 75 (1998): 159–173.

[24] R. Bruinsma. Electrostatics of DNA cationic lipid complexes: Isoelectric instability. *Eur. Phys. J. B* 4 (1998): 75–88.

[25] S. May, A. Ben-Shaul. Modeling of cationic lipid-DNA complexes. *Curr. Med. Chem.* 11 (2004): 151–167.

[26] T. Salditt, I. Koltover, J. O. Rädler, C. R. Safinya. Two-dimensional smectic ordering of linear DNA chains in self-assembled DNA–cationic liposome mixtures. *Phys. Rev. Lett.* 79 (1997): 2582–2585.

[27] J. O. Rädler, I. Koltover, A. Jamieson, T. Salditt, C. R. Safinya. Structure and interfacial aspects of self-assembled cationic lipid–DNA gene carrier complexes. *Langmuir* 14 (1998): 4272–4283.

[28] I. Koltover, T. Salditt, C. R. Safinya. Phase diagram, stability, and overcharging of lamellar cationic lipid–DNA self-assembled complexes. *Biophys. J.* 77 (1999): 915–924.

[29] I. Koltover, T. Salditt, J. O. Rädler, C. R. Safinya. An inverted hexagonal phase of cationic liposome–DNA complexes related to DNA release and delivery. *Science* 281 (1998): 78–81.

[30] A. J. Lin, N. L. Slack, A. Ahmad, C. X. George, C. E. Samuel, C. R. Safinya. Three-dimensional imaging of lipid gene-carriers: Membrane charge density controls universal transfection behavior in lamellar cationic liposome–DNA complexes. *Biophys. J.* 84 (2003): 3307.

[31] J. M. Seddon. Structure of the inverted hexagonal (H_{II}) phase, and non-lamellar phase transitions of lipids. *Biochim. Biophys. Acta* 1031 (1990): 1–69.

[32] N. Slack. Structure and Function Studies of Cationic Lipid Non-Viral Gene Delivery Systems. PhD dissertation University of California, Santa Barbara, CA, 2000.

[33] K. A. Mislick, J. D. Baldeschwieler. Evidence for the role of proteoglycans in cation-mediated gene transfer. *Proc. Natl. Acad. Sci. USA* 93 (1996): 12349–12354.

[34] L. C. Mounkes, W. Zhong, G. Ciprespalacin, T. D. Heath, R. J. Debs. Proteoglycans mediate cationic liposome-DNA complex-based gene delivery in vitro and in vivo. *J. Biol. Chem.* 273 (1998): 26164–26170.

[35] I. Kopatz, J. -S. Remy, J. -P. Behr. A model for non-viral gene delivery: Through syndecan adhesion molecules and powered by actin. *J. Gene Med.* 6 (2004): 769–776.

[36] M. T. McManus, P. A. Sharp. Gene silencing in mammals by small interfering RNAs. *Nat. Rev. Genet.* 3 (2002): 737–747.

[37] Y. Dorsett, T. Tuschl. siRNAs: Applications in functional genomics and potential as therapeutics. *Nat. Rev. Drug. Disc.* 3 (2004): 318–329.

[38] N. F. Bouxsein, C. S. McAllister, K. K. Ewert, C. E. Samuel, C. R. Safinya. Structure and gene silencing activities of monovalent and pentavalent cationic lipid vectors complexed with siRNA. *Biochemistry* 46 (2007): 4785–4792.

[39] G. C. L. Wong, J. X. Tang, A. Lin, Y. Li, P. A. Janmey, C. R. Safinya. Hierarchical self-assembly of F-actin and cationic lipid complexes: Stacked three-layer tubule networks. *Science* 288 (2000): 2035–2039.

[40] U. Raviv, D. J. Needleman, Y. Li, H. P. Miller, L. Wilson, C. R. Safinya. Cationic liposome–microtubule complexes: Pathways to the formation of two-state lipid–protein nanotubes with open or closed ends. *Proc. Natl. Acad. Sci. USA* 102 (2005): 11167–11172.

[41] D. Ferber. Gene therapy: Safer and virus-free? *Science* 294 (2001): 1638–1642.

[42] C. Plank, K. Mechtler, F. C. Szoka, E. Wagner. Activation of the complement system by synthetic DNA complexes: A potential barrier for intravenous gene delivery. *Human Gene Ther.* 7 (1996): 1437–1446.

[43] D. D. Lasic, D. Papahadjopoulos. Liposomes revisited. *Science* 267 (1995): 1275–1276.

[44] A. J. Bradley, D. V. Devine, S. M. Ansell, J. Janzen, D. E. Brooks. Inhibition of liposome-induced complement activation by incorporated poly(ethylene glycol) lipids. *Arch. Biochem. Biophys.* 357 (1998): 185–194.

[45] D. D. Lasic, F. J. Martin (Eds.). *Stealth liposomes*. CRC Press. Boca Raton, F L. 1995.

[46] M. C. Woodle. Sterically stabilized liposome therapeutics. *Adv. Drug Deliv. Rev.* 16 (1995): 249–265.

[47] A. Martin-Herranz, A. Ahmad, H. M. Evans, K. Ewert, U. Schulze, C. R. Safinya. Surface functionalized cationic lipid-DNA complexes for gene delivery: PEGylated lamellar complexes exhibit distinct DNA–DNA interaction regimes. *Biophys. J.* 86 (2004): 1160–1168.

[48] T. Salditt, I. Koltover, J. O. Rädler, C. R. Safinya. Self-assembled DNA-cationic-lipid complexes: Two-dimensional smectic ordering, correlations, and interactions. *Phys. Rev. E* 58 (1998): 889–904.

[49] V. V. Vasilevskaya, A. R. Khokhlov, Y. Matsuzawa, K. Yoshikawa. Collapse of single DNA molecule in poly(ethylene glycol) solutions. *J. Chem. Phys.* 102 (1995): 6595–6602.

[50] K. Devanand, J. C. Selser. Asymptotic-behavior and long-range interactions in aqueous-solutions of poly(ethylene oxide). *Macromolecules* 24 (1991): 5943–5947.

[51] H. E. Warriner, S. H. J. Idziak, N. L. Slack, P. Davidson, C. R. Safinya. Lamellar biogels: Fluid-membrane-based hydrogels containing polymer lipids. *Science* 271 (1996): 969–973.

[52] J. N. Israelachvili. *Intermolecular and Surface Forces*. Academic Press, London, 1992.

[53] P. Harvie, F. M. P. Wong, M. B. Bally. Use of poly(ethylene glycol)–lipid conjugates to regulate the surface attributes and transfection activity of lipid–DNA particles. *J. Pharm. Sci.* 89 (2000): 652–663.

[54] B. Pitard, N. Oudrhiri, O. Lambert, E. Vivien, C. Masson, B. Wetzer, M. Hauchecorne, D. Scherman, J. -L. Rigaud, J. -P. Vigneron, J. -M. Lehn, P. Lehn. Sterically stabilized BGTC-based lipoplexes: Structural features and gene transfection into the mouse airways in vivo. *J. Gene Med.* 3 (2001): 478–487.

[55] J. J. Wheeler, L. Palmer, M. Ossanlou, I. MacLachlan, R. W. Graham, Y. P. Zhang, M. J. Hope, P. Scherrer, P. R. Cullis. Stabilized plasmid-lipid particles: Construction and characterization. *Gene Ther.* 6 (1999): 271–281.